HHS Public Access

Author manuscript

Magn Reson Imaging Clin N Am. Author manuscript; available in PMC 2021 March 29.

Published in final edited form as:

Magn Reson Imaging Clin N Am. 2020 August ; 28(3): 353–367. doi:10.1016/j.mric.2020.03.003.

Advanced MR Imaging of the Pancreas

Danielle V. Hill, MD, **Temel Tirkes, MD***

Department of Radiology and Imaging Sciences, Indiana University School of Medicine, 550 North University Boulevard, Suite UH0663, Indianapolis, IN 46202, USA

Keywords

MRI; MRCP; T1 mapping; Extracellular volume; Diffusion-weighted imaging; Quantitative imaging

INTRODUCTION

MR imaging of the pancreas is a powerful tool to diagnose and characterize a range of anomalous and pathologic conditions such as variant ductal anatomy, inflammatory conditions such as chronic pancreatitis (CP), neoplasms, and ductal injuries. Because of the high functional reserve of the pancreas, early pathologic changes can be subtle, making diagnosis challenging.[1,2] In addition, interrogating the pancreas with endoscopic retrograde pancreatography (ERCP) or via tissue sampling carries complication risks, such as ERCPinduced pancreatitis. As a result, MR and MR cholangiopancreatography (MRCP) play major non invasive roles in identifying pancreatic pathologic condition with diagnostic power equivalent to ERCP.[1] Ductal detail can be enhanced by administration of secretin, thus improving the diagnostic capabilities of MRCP.[3,4] Technical innovations have continued to improve, now with most sequences being performed in a single or a few breath-holds, improving patient experience and decreasing motion artifact. As a result, MR has increasingly been used to evaluate the pancreas.[5] By using the current advanced capabilities of MR in conjunction with other imaging modalities, the radiologist is best equipped to diagnose a wide spectrum of pancreatic pathologic conditions. In this review article, the authors explore current MR imaging techniques.

MR SEQUENCES FOR PANCREAS IMAGING

A comprehensive MR examination should demonstrate detailed anatomy of the pancreatic duct and the biliary tree, detect and characterize parenchymal disease, delineate extension of neoplastic or inflammatory processes, and provide evaluation of the vascular anatomy. To do so, the following sequences may be used:

- T1-weighted gradient-echo
- T2-weighted axial and coronal sequences
- Turbo spin-echo (TSE) or a variant of TSE

*Corresponding author. atirkes@iupui.edu.

- Two-dimensional (2D) and 3-dimensional (3D) MRCP
- T1-weighted 3D gradient-echo before and after gadolinium (Gd)
- (optional) Secretin-enhanced MR cholangiopancreatography (S-MRCP)

Currently, it is possible to complete these core sequences within 30 minutes. Pancreatic imaging can adequately be performed with 1.5-T scanners, although 3.0 T is preferable for improved signal-to-noise ratio (SNR) if techniques such as parallel imaging and reconstruction algorithms are used to compensate for the potential decreased soft tissue contrast.[6-10] Tables 1 and 2 define the MR imaging parameters for these sequences on 1.5-T and 3.0-T scanners, respectively. Pancreatic pathologic conditions can be subtle in the early stages, for example, the loss of ductal compliance or subtle alterations in enhancement patterns that can be seen in early CP.[1] These parenchymal alterations, such as atrophy, loss of proteinaceous water content, and fibrotic changes, can be detected using advanced MR techniques, which include T1 signal intensity ratio (SIR), T1 mapping, diffusion-weighted imaging (DWI), elastography, and extracellular volume (ECV) quantification.

PREPARATION

Patient preparation is important, and fasting for at least 4 hours before the examination is recommended to ensure distention of the gallbladder. Administering a negative oral contrast agent is helpful to reduce fluid signal from the adjacent stomach and duodenum, which can obscure MRCP images. This is particularly necessary for adequate assessment of exocrine response if secretin is used. Pineapple or blueberry juice can be used as an oral contrast agent because the manganese content of these juices results in signal reduction on T2-weighted images.[11-13] Comparison of MRCP sequences without and then with negative oral contrast can be seen in Fig. 1. Motion artifact can markedly limit the yield of pancreatic MR imaging, especially detailed ductal views obtained on MRCP sequences, which are often too long to be performed with a single breath-hold. Therefore, efforts to minimize respiratory motion are necessary for optimal results. Techniques used during free breathing include the use of respiratory triggering, respiratory monitoring with navigator pulse (Fig. 2), and rotatory k-space sampling.

T2-WEIGHTED IMAGING

The normal pancreatic parenchyma exhibits relatively low to intermediate signal on T2-weighted images. These sequences are helpful in distinguishing fluid from solid tissue and to characterize cystic pancreatic lesions and evaluate pancreatic duct and peripancreatic inflammatory collections (Fig. 3). Because of the high signal from pancreatic fluid, the pancreatic duct is usually well delineated on T2 images, which can then be used to guide the acquisition of the MRCP series.[14]

FAT SUPPRESSION

Chemical shift fat suppression and inversion-recovery (IR) fat suppression are 2 approaches traditionally used to suppress fat. Chemical shift fat suppression exploits the difference of resonance frequency between fat and water. IR fat suppression, such as short tau inversion

recovery (STIR), relies on the difference in T1 relaxation times between fat and water. The fat signal is selectively suppressed by using an inversion time, generally 150 to 170 milliseconds for 1.5 T. IR techniques usually have more homogenous fat suppression and better contrast-to-noise ratio (CNR), but tend to have lower-spatial resolution or longer acquisition times. Spectral Adiabatic Inversion Recovery (SPAIR) is an IR fat-suppression technique whereby the inversion pulse is spectrally selective and only affects the fat protons. Compared with conventional IR, SPAIR generally has better SNR and reduced susceptibility artifact, notably at 3.0 T.[15]

Two-point Dixon method is an alternative technique that relies on the phase shifts created by the differences in fat-water resonance frequency to separate water from fat. A fast spin echo (FSE) T2-weighted 2-point Dixon sequence can reduce overall scan time by generating both T2 and fat-suppressed T2-weighted images during a single acquisition. A study aimed at quantifying pancreatic steatosis and fibrosis with histologic analysis found a moderate correlation of MR fat fractions using the T2*-corrected Dixon technique.[16] Pre-liminary testing of flexible FSE triple-echo Dixon technique shows promise in combining the effi-ciency of FSE and reliable separation of fat and water in Dixon imaging.[17]

MR CHOLANGIOPANCREATOGRAPHY IMAGING

MRCP is a noninvasive technique for evaluating the pancreatic ducts with similar diagnostic accuracy to ERCP.[18] It relies on acquisition of heavily T2-weighted images to provide noninvasive detailed evaluation of the pancreaticobiliary ductal system.[1] For example, MRCP has traditionally been used to diagnose and grade severity of CP by comparing ductal imaging with the Cambridge classification developed for ERCP grading (Fig. 4). Although this has proved to have similar efficacy to ERCP, further diagnostic criteria are necessary to include the parenchymal changes that occur early in the course of CP, thus providing opportunity for earlier intervention. A large multiinstitutional study is underway aimed at producing a radiologic-based scoring system to serve as a biomarker for pancreatic fibrosis and possibly to grade efficacy of therapeutic agents on the progression or reversal of disease.[19]

Secretin-Enhanced–MR Cholangiopancreatography

The addition of secretin during MRCP can improve visualization of the pancreatic duct and is particularly helpful in evaluating congenital anomalies (Fig. 5), in evaluating cystic pancreatic tumors, and in assessing acute pancreatitis (AP) and Cp.[4,18,20-22] Administration of secretin for example, ChiRhoStim; ChiRhoClin Inc, Burtonsville, MD, USA; Secrelux, Sanochemia results in secretion of pancreatic fluid from acinar cells and simultaneous increased tone of the sphincter of Oddi. As a result, there is increased dilatation and visualization of the pancreatic duct that improves the diagnostic yield of MRCP.[3,4] This effect can result in distention of the duct by 1 mm or more and usually peaks after 3 to 5 minutes following injection.[23] Lack of main duct distensibility can be thought of as a surrogate for noncompliance secondary to periductal fibrosis seen with CP.[24] The degree to which the pancreas is able to respond to secretin can also be used to estimate loss of pancreatic function, be it from an inflammatory process or after pancreatoduodenectomy.[4]

Exocrine response of the pancreas is routinely evaluated semiquantitatively by assessing duodenal filling with grade 1 to 4 corresponding to the segment of duodenum the secreted fluid extends to (ie, grade 1 equates to fluid in the duodenal bulb and grade 4 when fluid is seen reaching the fourth segment of the duodenum).[4,24]

Three-Dimensional MR Cholangiopancreatography

3D TSE sequence can produce high-spatial resolution MRCP images with thin sections, which can be useful for detecting small stones, evaluating the intrahepatic ducts, and imaging ductal side branches.[25,26] A 3D TSE sequence can be performed either during free breathing and using motion reduction techniques or as a series of breath-holds. The disadvantage of free breathing is the relatively long acquisition time and need for uniform, regular breathing cycles. Another option for producing 3D MRCP images is the use of a TSE sequence with the addition of a 90° flipback pulse known as a fast recovery fast spin-echo, DRIVE, or RESTORE. The advantage of these sequences is their ability to reduce repetition time (TR) while maintaining SNR and is done by refocusing of the residual transverse magnetization after a long echo train, which is then flipped along the z-axis by a −90° fast-recovery pulse, thereby accelerating the relaxation of the longitudinal magnetization.[25,27]

FLIP ANGLE MODULATION

Traditional 3D MRCP used a constant flip angle to generate images, which at 1.5 T does not generate significant energy deposition. With the increasing use of 3-T scanners, however, this technique generates a high amount of radiofrequency (RF) energy. Flip-angle modulation techniques generate 3D TSE sequences using variable flip angles (VFA), thus significantly reducing the specific absorption rate, perhaps as much as 70%.[28] In addition, variable flip-angle techniques can maintain higher signal intensity (SI) in a long echo train, thus producing higher SNR.[29] Example techniques include SPACE (Sampling Perfection with Application optimized Contrasts using different flip angle Evolutions), XETA (Extended Echo Train Acquisition), and CUBE (not an acronym).

T1-WEIGHTED IMAGING

The pancreatic parenchyma has a shorter T1 relaxation time compared with other intraabdominal organs because of protein-rich acinar cells.[30] As a result, the normal pancreas is relatively hyperintense on unenhanced T1-weighted images. Decreased T1 signal is indicative of loss of acinar cells, which are replaced with fibrosis, especially in CP.[31] The degree of signal loss can be assessed by comparing the brightness of the pancreas on unenhanced T1-weighted images with a reference organ, such as the spleen or paraspinal muscles. The SI can be further quantified by calculating the SIR, which is found by dividing the average SI of the pancreas with the reference organ of choice (spleen or paraspinal muscle); SIR = $SI_{Pancreas}/SI_{Reference}$.[1] A decreased SIR between the pancreas and muscle was found to correlate with increased parenchymal fibrosis in patients who underwent pancreatectomy.[30] Another study found a significant difference in SNR between pancreas and spleen comparing normal and low pancreatic fluid bicarbonate groups. There was also a significant correlation between pancreatic fluid bicarbonate fluid level and SIR of pancreas

compared with spleen.[32] Furthermore, the normal hyperintense signal of the pancreas on unenhanced T1 images can be used to delineate nonpancreatic tissue, such as some pancreatic neoplasms, and can be especially helpful for pancreatic adenocarcinoma (PDAC), whereby the tumor is typically hypointense to normal pancreas on T1-weighted fat-suppressed sequences[33] (Fig. 6). However, a known mimic of pancreatic tumors includes confined areas of inflammation, such as in mass-forming CP, which can also result in hypointense SI on T1-weighted images.[34,35] Although the clinical background for both entities can be similar, features including the duct-penetrating sign and concurrent collateral duct dilatation are usually indicators of mass-forming pancreatitis, best assessed on S-MRCP.[35-37]

CONTRAST-ENHANCED T1-WEIGHTED IMAGING

Gd increases the T1 SI of normal pancreatic parenchyma, aiding in the detection of pancreatic lesions. For example, pancreatic neuroendocrine tumors are typically hypointense compared with normal pancreas on unenhanced fat-suppressed T1-weighted images but show hypervascular enhancement during the arterial phase[38] (Fig. 7A, B). Enhancement of the normal pancreatic parenchyma can increase visualization of PDAC, which usually demonstrates decreased enhancement on arterial phase with progressive enhancement on delayed phases.[38] Therefore, acquisition of Gd-enhanced sequences is advisable unless contraindicated (ie, severe allergy, pregnancy, and end-stage renal dysfunction). A 3D fat-suppressed spoiled gradient echo is the sequence of choice for pre-Gd and post-Gd series. A few common examples include volume interpolated breath-hold fast gradient echo, live acquisition with volume acceleration, and T1-weighted high-resolution isotropic volume examination. The entire pancreas and liver are typically included and imaged in multiple phases (arterial, venous, and delayed) after injecting Gd through a power injector at 2 mL/s followed by a 20-mL saline flush. Acquisition can usually be performed in a 20-s breath-hold providing 2 to 5 mm contiguous slices through the upper abdomen. Timing of the bolus can be performed using fixed time delays such as 25, 60, and 180 seconds, respectively, or with bolus tracking. Fixed time delays may be adequate in patients without cardiovascular comorbidities.[39] However, bolus tracking gives a more reliable arterial phase in patients with comorbidities, such as hypertension or cirrhosis.[40] At the authors' institution, a bolus tracking sequence is used to monitor the distal aorta at the diaphragmatic hiatus. Once contrast appears, the patient is given breathing instructions, and the arterial phase is initiated 8 seconds later. A quality arterial phase should demonstrate contrast predominantly in the aorta and superior mesenteric artery with some contrast seen in the portal vein. No contrast should be seen in the hepatic veins. Clear instructions and coaching on breath-holds from the technologist are necessary to reduce motion artifact.

DYNAMIC CONTRAST-ENHANCED MR IMAGING

Dynamic contrast-enhanced MR imaging requires a rapid sequence of images with high temporal resolution to analyze the dynamic uptake and subsequent washout of a contrast agent. It is frequently used for abdominal applications to demonstrate the changes in tissue SI over time after contrast administration and can help differentiate lesions with differing perfusion characteristics or measure pancreatic blood flow. Other MR perfusion techniques

include dynamic susceptibility contrast and arterial spin labeling. Both techniques are used in neuroradiology, but few sources are found discussing their use in pancreatic imaging.[41-43]

T1 MAPPING

Many studies have shown that pancreatic fibrosis causes T1 relaxation time to increase, thus decreasing the normal T1 hyperintense signal of the pancreas. T1 mapping is a quantitative MR imaging technique allowing measurement of tissue-specific T1 relaxation time. Once limited in abdominal application because of long scan times inherent in spin-echo imaging, newer protocols using 3D VFA gradient echo and parallel imaging techniques can produce parametric maps of T1 relaxation time in a single breath-hold. An advantage of new T1 mapping techniques is its decreased acquisition time compared with other techniques, such as DWI or S-MRCP.

Pancreatic parenchyma has a median T1 of 654 milliseconds at 1.5 T and a median T1 of 717 milliseconds at 3.0 T.[44] Quantification of the data allows for ready comparison across longitudinal time points as well as population-derived norms, offering the potential benefit of using quantitative MR imaging as a biomarker for a spectrum of diseases. For example, comparing T1 relaxation time of pancreatic tissue in normal controls and in patients with mild CP, a statistically significant increase of T1 relaxation time was found in the group with mild CP (Fig. 8). Sensitivity of 80% and 69% specificity for mild CP was found using a T1 relaxation time cutoff of 900 milliseconds at 3 T.[45] However, more studies are required to reach a consensus on what the normal T1 of abdominal organs should be and the amount of signal change necessary to diagnose clinically significant pathologic condition.[1]

There are multiple T1 mapping pulse sequence products or prototypes under development by manufacturers, although there is no consensus yet on which sequence is ideal for abdominal imaging. That said, a recent study compared 4 different pulse sequences: VFA, modified look-locker inversion recovery (MOLLI), a prototype inversion recovery snapshot, and a prototype saturation recovery single-shot acquisition (SASHA).[46] VFA pulse sequence quantifies T1 by acquiring voxel signals at steady state by using multiple flip angles.[47] Inversion recovery snapshot relies on the relaxation of longitudinal magnetization after an inversion RF pulse is applied. With this sequence, after the inversion RF pulse, a series of quick acquisitions are collected at different delay times and are fitted using the relaxation model.[48] MOLLI is a commercially available sequence originally developed for myocardial imaging and uses a modified variation of inversion recovery snapshot. The acquisitions following the inversion RF are segmented and synchronized using ECG signal with the data acquisition only occurring during diastole.[49] SASHA is also similar to inversion recovery snapshot; however, it uses a saturation RF instead of an inversion RF pulse.[50] The study found MOLLI, SASHA, and inversion recovery snapshot had the highest precision, whereas VFA has relatively less, although still substantial, precision. Because MOLLI and SASHA were designed for myocardial imaging, they provide a single image per breath-hold, whereas inversion recovery snapshot can acquire 3 images. In either case, this is potentially problematic because the pancreas may shift in location with each breath-hold. VFA, on the other hand, can generate fast 3D acquisition of 64 slices in a single breath-hold. However, VFA is inherently sensitive to pulsatile flow within the aorta. Ultimately, the study

concluded more refinement of these pulse sequences is necessary to provide the high precision and large spatial coverage needed during 1 breath-hold optimal for abdominal imaging.[44]

DIFFUSION-WEIGHTED IMAGING

DWI is used to identify areas where there is reduced mobility of water molecules. With the development of "ultrafast" echoplanar and parallel imaging in combination with improvements in high-density surface coils and respiratory navigation, the role of DW imaging in the body has expanded.[51,52] In the pancreas, this can aid in diagnosing tumors (Fig. 7C, D) and inflammation. A study found patients with AP had significantly lower apparent diffusion coefficient (ADC) values compared with normal pancreatic parenchyma.[53] DWI is a spin-echo T2-weighted sequence that uses a pair of gradients applied before and after a 180° refocusing RF pulse to measure the diffusivity of tissue. Restriction of water molecules produces imaging with high SI on the DW images and low signal on the ADC maps. The phase shift caused by the initial gradient is canceled by the second gradient, and thus, there is no significant loss of signal.[54,55] When water molecules move freely, the movement between the first and second gradient results in decreased signal on DWI. Practically, this results in high SI on both the DW images and the ADC maps, although the signal decreases at higher b values.

EXTRACELLULAR VOLUME IMAGING

ECV imaging is a quantitative MR radiomics tool that calculates increased extracellular matrix secondary to tissue fibrosis, namely, collagen[56,57] and proteoglycan content.[58] Although changes to the extracellular matrix can be seen in a variety of intraabdominal pathologic conditions, in the pancreas, it can be used as a marker for CP.[45,59] Using Gd as an extracellular contrast agent, the ECV dichotomizes pancreatic tissue into intracellular and extracellular/interstitial spaces. ECV fractions can then be depicted as pixels on an image called ECV map. To do so, tissue and blood plasma concentrations of Gd are compared by uing the T1 relaxation times obtained from the pancreas and the aortic lumen (blood pool) in unenhanced and postcontrast equilibrium phases.

These values are then calculated by the following formula:

$$\mathrm{ECV}_{\mathrm{pancreas}} = \frac{(1 - \mathrm{hematocrit}) \times \Delta \mathrm{R1}_{\mathrm{pancreas}}}{\Delta \mathrm{R1}_{\mathrm{blood}}}$$

where $\Delta R1$ pancreas and $\Delta R1$ blood are defined as the change of $1/T_1$ relaxation rate in pancreas and blood pool relaxivity before and after contrast administration; T_1 is a time constant describing the longitudinal relaxation rate; and its reciprocal ($1/T_1$) is referred to as $R1$. The change in $R1$ ($\Delta R1$) is defined as: ΔR1 = (R1postcontrast) – (R1 precontrast). $\Delta R1$ is proportional to Gd concentration when both tissues are in equilibrium; $\Delta R1_{\mathrm{pancreas}}/\Delta R1_{\mathrm{blood}} = [\mathrm{Gd}]_{\mathrm{pancreas}}/[\mathrm{Gd}]_{\mathrm{blood}}$. Because the Gd chelates are extracellular agents, the ratio of contrast agent concentrations between the pancreas and blood equals the ratio of ECV between the tissues: $[\mathrm{Gd}]_{\mathrm{pancreas}}/[\mathrm{Gd}]_{\mathrm{blood}} =$"' $\mathrm{ECV}_{\mathrm{pancreas}}/\mathrm{ECV}_{\mathrm{blood}}$. The ECV of the blood

is defined as the fraction of the blood volume, which is not composed of blood cells (ie, the fraction of plasma). The plasma volume is simply calculated as ECV_{blood} = [1 – hematocrit].[59]

The pancreas has a reported median ECV of 0.28 on 1.5 T (interquartile range [IQR]: 0.21–0.33), and median ECV of 0.25 (IQR 0.19–0.28) on 3.0 T.[44] A study by Tirkes and colleagues,[59] investigating patients with and without known pancreatic disease, reported that an ECV greater than 0.27 demonstrated 92% sensitivity and 77% specificity for the diagnosis of CP when using a 3.0-T scanner (Fig. 9). By combining ECV and T1, this study achieved 85% sensitivity and 92% specificity for diagnosing mild CP (area under the curve: 0.94).[59] Although T1 relaxation times differ between 1.5 T and 3 T, ECV fractions are similar in different magnet strengths.

MR ELASTOGRAPHY

Increased stiffness of the pancreas indicates fibrosis and can be found in CP (Figs. 10 and 11) as well as in pancreatic cancer.[60] MR elastography (MRE) of the liver is a very useful tool in evaluating the degree of hepatic fibrosis; however, MRE of the pancreas is still under development.[61] A pilot study of 20 healthy volunteers who underwent MRE examinations demonstrated promising and reproducible stiffness measurements throughout the pancreas.[62] In the study, an experimental MRE driver that emitted lower-frequency vibrations in order to reach the deeper location of the pancreas was used. Mean shear stiffness was found to be (1.15 ± 0.17) kPa at 40 Hz and (2.09 ± 0.33) kPa at 60 Hz.[62] Another pilot study of healthy volunteers also showed highly reproducible pancreatic stiffness measurements with a linear increase in stiffness with age.[63] In both preliminary studies, 3D spin-echo echo planar imaging sequence was used to obtain 3D wave information along with 3D spatial data.

PANCREATIC FAT FRACTION

MR is superior at detecting fat deposition in tissues compared with computed tomography (CT) and ultrasound. There are multiple tools for quantifying fat using Web-based calculators as well as vendor software packages. Similarly, quantifying fat within the pancreas can be performed; however, more data are needed to establish a consensus on the normal range of pancreatic fat fraction. A study performed on a large healthy volunteer population in Europe reported the normal pancreatic fat fraction as 4.4%.[64] In the United States, the fat fraction in the general population is reported to be between 8.3%[45] and 15%.[65] There appears to be an association with CP and a higher pancreatic fat fraction and higher visceral adipose tissue.[65] This topic is underinvestigated, and further research is needed to examine the clinical consequences of pancreatic steatosis.

Chemical shift imaging techniques depend on the different resonance frequencies of water and fat protons. Two-point Dixon method is a practical technique with excellent image resolution routinely used to obtain T1-weighted in-phase, out-of-phase, water-only, and fat-only images as discussed above. From these sequences, the pancreatic fat signal fraction (FSF) can be calculated from measuring SI in localized regions of interest:

$$FSF = SI_{fat} / SI_{fat} + SI_{water}$$

Alternatively, newer MR software can produce a quantitative proton density fat fraction (PDFF) map by using more complex, multiecho acquisition sequences. T1 bias and T2* correction should be used to ensure a reliable assessment of quantitative fat.[66,67] PDFF map shows promise as a biomarker for estimating the probability of pancreatic cancer. In a study comparing PDFF map with pancreatic index using CT, comparison of pancreatic and splenic tissue with histologic results in patients with pancreatic cancer demonstrated PDFF map was significantly higher along with higher histologic fat fraction for the cancer group.[68]

SUMMARY

Despite the challenges inherent in pancreatic imaging, multiple MR imaging tools can optimize detail and increase diagnostic yield for a range of pancreatic pathologic condition and variant anatomy. In addition to the traditional MR sequences, several emerging sequences, such as T1 mapping, ECV fraction, DWI, and recently, pancreas MRE, show promise for earlier disease detection and quantitative analysis of the pancreas. T1 mapping provides quantitative measurement of the T1 relaxation time of tissue and may be useful in identifying CP, including at the early stage. ECV quantifies the extracellular space (which is increased with tissue fibrosis). Restricted movement of water molecules demonstrated on DWI may aid in detecting neoplastic and inflammatory processes. FSF imaging can quantify the degree of pancreatic steatosis, which increases in patients with CP.

Acknowledgments

Dr T. Tirkes is supported by National Cancer Institute and National Institute of Diabetes and Digestive and Kidney Diseases of the National Institutes of Health under award numbers 1R01DK116963 and U01DK108323 (Consortium for the Study of Chronic Pancreatitis, Diabetes, and Pancreatic Cancer). The content is solely the responsibility of the authors and does not necessarily represent the official views of the National Institutes of Health.

REFERENCES

1. Parakh A, Tirkes T. Advanced imaging techniques for chronic pancreatitis. Abdom Radiol (N Y) 2020; 45(5): 1420–38.
2. Pansky B Anatomy of the pancreas. Emphasis on blood supply and lymphatic drainage. Int J Pancreatol 1990; 7(1–3): 101–8. [PubMed: 2081913]
3. Carbognin G, et al. Collateral branches IPMTs: secretin-enhanced MRCP. Abdom Imaging 2007; 32(3):374–80. [PubMed: 16967247]
4. Tirkes T, et al. Secretin-enhanced MR cholangiopancreatography: spectrum of findings. Radiographics 2013;33(7): 1889–906. [PubMed: 24224585]
5. Tirkes T, Menias CO, Sandrasegaran K. MR imaging techniques for pancreas. Radiol Clin North Am 2012; 50(3):379–93. [PubMed: 22560687]
6. Erturk SM, et al. Use of 3.0-T MR imaging for evaluation of the abdomen. Radiographics 2009;29(6): 1547–63. [PubMed: 19959507]
7. Soher BJ, Dale BM, Merkle EM. A review of MR physics: 3T versus 1.5T. Magn Reson Imaging Clin N Am 2007; 15(3) :277–90, v. [PubMed: 17893049]
8. de Bazelaire CM, et al. MR imaging relaxation times of abdominal and pelvic tissues measured in vivo at 3.0 T: preliminary results. Radiology 2004;230(3):652–9. [PubMed: 14990831]

9. Chang KJ, et al. 3.0-T MR imaging of the abdomen: comparison with 1.5 T. Radiographics 2008;28(7): 1983–98. [PubMed: 19001653]
10. Akisik FM, et al. Abdominal MR imaging at 3.0 T. Radiographics 2007;27(5):1433–44 [discussion: 1462–4]. [PubMed: 17848701]
11. Coppens E, et al. Pineapple juice labeled with gadolinium: a convenient oral contrast for magnetic resonance cholangiopancreatography. Eur Radiol 2005; 15(10): 2122–9. [PubMed: 15999215]
12. Papanikolaou N, et al. MR cholangiopancreatography before and after oral blueberry juice administration. J Comput Assist Tomogr 2000;24(2):229–34. [PubMed: 10752883]
13. Riordan RD, et al. Pineapple juice as a negative oral contrast agent in magnetic resonance cholangiopancreatography: a preliminary evaluation. Br J Radiol 2004; 77(924):991–9. [PubMed: 15569640]
14. Matos C, et al. MR imaging of the pancreas: a pictorial tour. Radiographics 2002;22(1):e2. [PubMed: 11796914]
15. Lauenstein TC, et al. Evaluation of optimized inversion-recovery fat-suppression techniques for T2-weighted abdominal MR imaging. J Magn Reson Imaging 2008;27(6):1448–54. [PubMed: 18504735]
16. Yoon JH, et al. Pancreatic steatosis and fibrosis: quantitative assessment with preoperative multiparametric MR imaging. Radiology 2016;279(1): 140–50. [PubMed: 26566228]
17. Son JB, et al. A flexible fast spin echo triple-echo Dixon technique. Magn Reson Med 2017;77(3): 1049–57. [PubMed: 26982770]
18. Akisik MF, et al. Dynamic secretin-enhanced MR cholangiopancreatography. Radiographics 2006; 26(3):665–77. [PubMed: 16702446]
19. Tirkes T, et al. Magnetic resonance imaging as a non-invasive method for the assessment of pancreatic fibrosis (MINIMAP): a comprehensive study design from the consortium for the study of chronic pancreatitis, diabetes, and pancreatic cancer. Abdom Radiol (N Y) 2019;44(8):2809–21.
20. Patel FIT, et al. MR cholangiopancreatography at 3.0 T. Radiographics 2009;29(6):1689–706. [PubMed: 19959516]
21. Manfredi R, et al. Severe chronic pancreatitis versus suspected pancreatic disease: dynamic MR cholangiopancreatography after secretin stimulation. Radiology 2000;214(3):849–55. [PubMed: 10715057]
22. Sandrasegaran K, et al. The value of secretin-enhanced MRCP in patients with recurrent acute pancreatitis. AJR Am J Roentgenol 2017;208(2): 315–21. [PubMed: 27824485]
23. Matos C, et al. Pancreatic duct: morphologic and functional evaluation with dynamic MR pancreatography after secretin stimulation. Radiology 1997; 203(2):435–41. [PubMed: 9114101]
24. Cappeliez O, et al. Chronic pancreatitis: evaluation of pancreatic exocrine function with MR pancreatography after secretin stimulation. Radiology 2000; 215(2):358–64. [PubMed: 10796908]
25. Sodickson A, et al. Three-dimensional fast-recovery fast spin-echo MRCP: comparison with two-dimensional single-shot fast spin-echo techniques. Radiology 2006;238(2):549–59. [PubMed: 16436816]
26. Yoon LS, et al. Another dimension in magnetic resonance cholangiopancreatography: comparison of 2- and 3-dimensional magnetic resonance cholangiopancreatography for the evaluation of intraductal papillary mucinous neoplasm of the pancreas. J Comput Assist Tomogr 2009;33(3): 363–8. [PubMed: 19478628]
27. Busse RF, et al. Interactive fast spin-echo imaging. Magn Reson Med 2000;44(3):339–48. [PubMed: 10975883]
28. Weigel M, Hennig J. Contrast behavior and relaxation effects of conventional and hyperecho-turbo spin echo sequences at 1.5 and 3 T. Magn Reson Med 2006;55(4):826–35. [PubMed: 16463351]
29. Arizono S, et al. High-spatial-resolution three-dimensional MR cholangiography using a highsampling-efficiency technique (SPACE) at 3T: comparison with the conventional constant flip angle sequence in healthy volunteers. J Magn Reson Imaging 2008;28(3):685–90. [PubMed: 18777552]
30. Watanabe H, et al. Fibrosis and postoperative fistula of the pancreas: correlation with MR imaging findings–preliminary results. Radiology 2014;270(3): 791–9. [PubMed: 24475834]

31. Ammann RW, Heitz PU, Kloppel G. Course of alcoholic chronic pancreatitis: a prospective clinicomorphological long-term study. Gastroenterology 1996; 111(1):224–31. [PubMed: 8698203]
32. Tirkes T, et al. Detection of exocrine dysfunction by MRI in patients with early chronic pancreatitis. Abdom Radiol (N Y) 2017;42(2):544–51.
33. Miller FH, Rini NJ, Keppke AL. MRI of adenocarcinoma of the pancreas. AJR Am J Roentgenol 2006;187(4):W365–74. [PubMed: 16985107]
34. Momtahen AJ, et al. Focal pancreatitis mimicking pancreatic mass: magnetic resonance imaging (MRI)/magnetic resonance cholangiopancreatography (MRCP) findings including diffusion-weighted MRI. Acta Radiol 2008;49(5):490–7. [PubMed: 18568532]
35. Wolske KM, et al. Chronic pancreatitis or pancreatic tumor? A problem-solving approach. Radiographics 2019;39(7): 1965–82. [PubMed: 31584860]
36. Ichikawa T, et al. Duct-penetrating sign at MRCP: usefulness for differentiating inflammatory pancreatic mass from pancreatic carcinomas. Radiology 2001; 221 (1): 107–16. [PubMed: 11568327]
37. Siddiqui N, et al. Advanced MR imaging techniques for pancreas imaging. Magn Reson Imaging Clin N Am 2018;26(3):323–44. [PubMed: 30376973]
38. Wang Y, et al. Diffusion-weighted MR imaging of solid and cystic lesions of the pancreas. Radiographics 2011;31(3):E47–64. [PubMed: 21721197]
39. Materne R, et al. Gadolinium-enhanced arterialphase MR imaging of hypervascular liver tumors: comparison between tailored and fixed scanning delays in the same patients. J Magn Reson Imaging 2000; 11(3):244–9. [PubMed: 10739555]
40. Sharma P, et al. Gadolinium-enhanced imaging of liver tumors and manifestations of hepatitis: pharmacodynamic and technical considerations. Top Magn Reson Imaging 2009;20(2):71–8. [PubMed: 20010061]
41. Taso M, et al. Pancreatic perfusion modulation following glucose stimulation assessed by noninvasive arterial spin labeling (ASL) MRI. J Magn Reson Imaging 2020;51(3):854–60. [PubMed: 31410924]
42. Schraml C, et al. Perfusion imaging of the pancreas using an arterial spin labeling technique. J Magn Reson Imaging 2008;28(6):1459–65. [PubMed: 19025955]
43. Niwa T, et al. Dynamic susceptibility contrast MRI in advanced pancreatic cancer: semi-automated analysis to predict response to chemotherapy. NMR Biomed 2010;23(4):347–52. [PubMed: 19950116]
44. Tirkes T, et al. Normal T1 relaxometry and extracellular volume of the pancreas in subjects with no pancreas disease: correlation with age and gender. Abdom Radiol (N Y) 2019;44(9):3133–8.
45. Tirkes T, et al. T1 mapping for diagnosis of mild chronic pancreatitis. J Magn Reson Imaging 2017; 45(4): 1171–6. [PubMed: 27519287]
46. Tirkes T, et al. Evaluation of variable flip angle, MOLLI, SASHA, and IR-SNAPSHOT pulse sequences for T1 relaxometry and extracellular volume imaging of the pancreas and liver. MAGMA 2019; 32(5):559–66. [PubMed: 31165353]
47. Cheng HL, Wright GA. Rapid high-resolution T(1) mapping by variable flip angles: accurate and precise measurements in the presence of radiofrequency field inhomogeneity. Magn Reson Med 2006;55(3):566–74. [PubMed: 16450365]
48. Nekolla S, et al. T1 maps by K-space reduced SNAPSHOT-FLASH MRI. J Comput Assist Tomogr 1992;16(2):327–32. [PubMed: 1545039]
49. Messroghli DR, et al. Modified Look-Locker inversion recovery (MOLLI) for high-resolution T1 mapping of the heart. Magn Reson Med 2004;52(1):141–6. [PubMed: 15236377]
50. Datta S, et al. Distinct distribution pattern of hepatitis B virus genotype C and D in liver tissue and serum of dual genotype infected liver cirrhosis and hepatocellular carcinoma patients. PLoS One 2014;9(7): e102573. [PubMed: 25032957]
51. Ichikawa T, et al. Diffusion-weighted MR imaging with single-shot echo-planar imaging in the upper abdomen: preliminary clinical experience in 61 patients. Abdom Imaging 1999;24(5):456–61. [PubMed: 10475927]

52. Kanematsu M, et al. Diffusion/perfusion MR imaging of the liver: practice, challenges, and future. Magn Reson Med Sci 2012;11(3):151–61. [PubMed: 23037559]
53. Thomas S, et al. Diffusion MRI of acute pancreatitis and comparison with normal individuals using ADC values. Emerg Radiol 2012;19(1):5–9. [PubMed: 21927794]
54. Barral M, et al. Diffusion-weighted MR imaging of the pancreas: current status and recommendations. Radiology 2015;274(1):45–63. [PubMed: 25531479]
55. Koh DM, Collins DJ. Diffusion-weighted MRI in the body: applications and challenges in oncology. AJR Am J Roentgenol 2007;188(6): 1622–35. [PubMed: 17515386]
56. Haber PS, et al. Activation of pancreatic stellate cells in human and experimental pancreatic fibrosis. Am J Pathol 1999;155(4): 1087–95. [PubMed: 10514391]
57. Charrier AL, Brigstock DR. Connective tissue growth factor production by activated pancreatic stellate cells in mouse alcoholic chronic pancreatitis. Lab Invest 2010;90(8):1179–88. [PubMed: 20368699]
58. Pan S, et al. Proteomics portrait of archival lesions of chronic pancreatitis. PLoS One 2011;6(11): e27574. [PubMed: 22132114]
59. Tirkes T, et al. Quantitative MR evaluation of chronic pancreatitis: extracellular volume fraction and MR relaxometry. AJR Am J Roentgenol 2018;210(3): 533–42. [PubMed: 29336598]
60. An H, et al. Test-retest reliability of 3D EPI MR elastography of the pancreas. Clin Radiol 2016;71(10): 1068.e7–12.
61. Wang Y, et al. Assessment of chronic hepatitis and fibrosis: comparison of MR elastography and diffusion-weighted imaging. AJR Am J Roentgenol 2011;196(3):553–61. [PubMed: 21343496]
62. Shi Y, et al. Feasibility of using 3D MR elastography to determine pancreatic stiffness in healthy volunteers. J Magn Reson Imaging 2015;41(2):369–75. [PubMed: 24497052]
63. Kolipaka A, et al. Magnetic resonance elastography of the pancreas: measurement reproducibility and relationship with age. Magn Reson Imaging 2017; 42:1–7. [PubMed: 28476308]
64. Kuhn JP, et al. Pancreatic steatosis demonstrated at MR imaging in the general population: clinical relevance. Radiology 2015;276(1):129–36. [PubMed: 25658037]
65. Tirkes T, et al. Association of pancreatic steatosis with chronic pancreatitis, obesity, and type 2 diabetes mellitus. Pancreas 2019;48(3):420–6. [PubMed: 30747825]
66. Kang GH, et al. Reproducibility of MRI-determined proton density fat fraction across two different MR scanner platforms. J Magn Reson Imaging 2011;34(4):928–34. [PubMed: 21769986]
67. Schwenzer NF, et al. Quantification of pancreatic lipomatosis and liver steatosis by MRI: comparison of in/opposed-phase and spectral-spatial excitation techniques. Invest Radiol 2008;43(5): 330–7. [PubMed: 18424954]
68. Fukui H, et al. Evaluation of fatty pancreas by proton density fat fraction using 3-T magnetic resonance imaging and its association with pancreatic cancer. Eur J Radiol 2019;118: 25–31. [PubMed: 31439250]

KEY POINTS

- T2-weighted imaging is useful for assessing fluid components of lesions or collections and provides guidance for MR cholangiopancreatography (MRCP) acquisition.
- MRCP sequences provide detailed images of the pancreatic duct and can be further augmented with secretin to improve visualization and grade the exocrine function of the pancreas.
- T1-weighted images are useful in assessing the pancreatic parenchyma, detecting areas of hemorrhage, and characterizing the enhancement pattern of neoplasms after gadolinium administration.
- Advanced imaging techniques, such as T1 mapping, diffusion-weighted imaging, elastography, and extracellular volume quantification, show promise for adding diagnostic value and further data quantification.

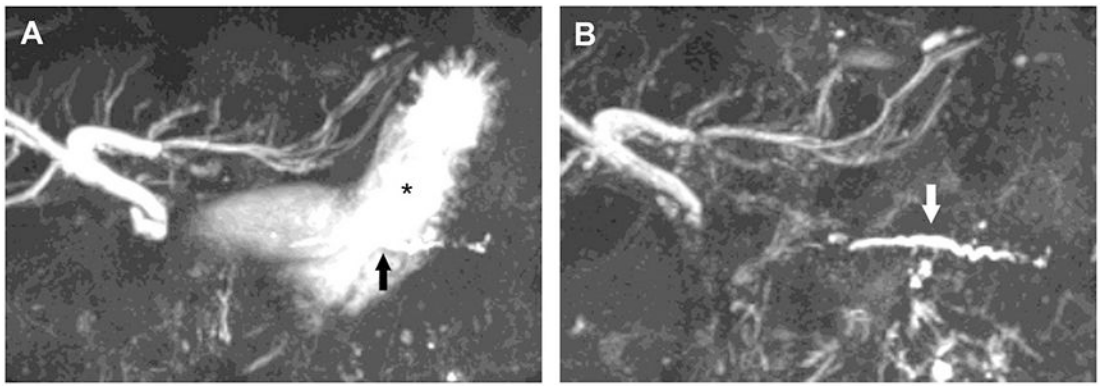

Fig. 1.

A 65-year-old patient with a history of intraductal papillary mucinous neoplasm, status post Whipple operation. (*A*) Coronal MRCP image with hyperintense signal from fluid within the stomach (*asterisk*), which obscures the body and tail of the pancreas as well as the cystic lesion (*black arrow*). (*B*) Same patient reexamined after ingesting a negative contrast agent, thus nullifying the signal from the stomach. Repeat study shows good visualization of the cystic mass and the main pancreatic duct (*arrow*). (*From* Tirkes T, Menias CO, Sandrasegaran K. MR imaging techniques for pancreas. Radiol Clin North Am 2012;50(3):382; with permission.)

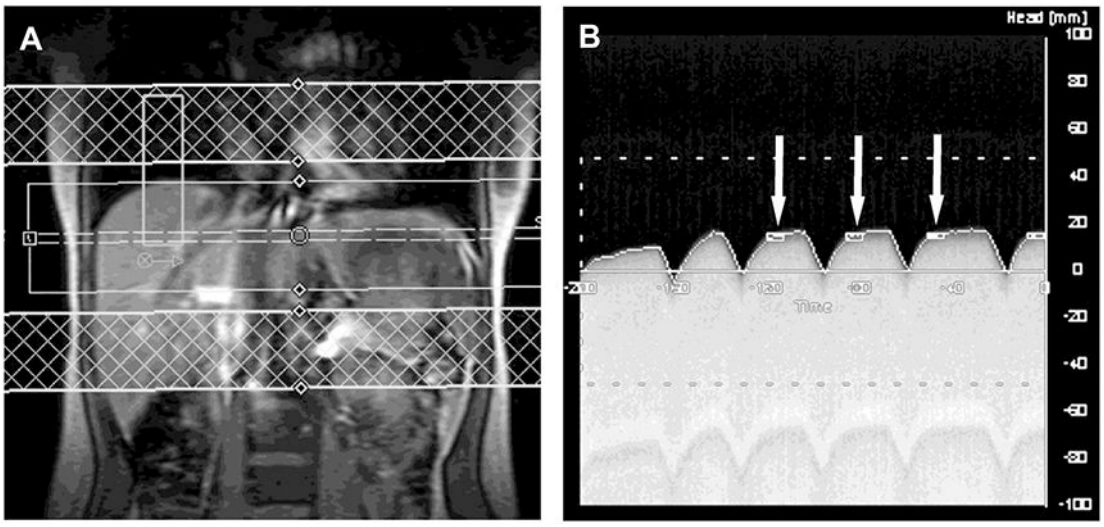

Fig. 2.

Navigator monitoring of respiratory motion. (*A*) First, a coronal 2D, low-resolution gradient-echo image with small flip angle is acquired. (*B*) The respiratory motion of the right hemidiaphragm is traced in real time with subsequent synchronization of the data with the patient's respiratory cycle. Initially, the range of motion is determined, and then on subsequent respirations, data acquisition is triggered when the diaphragm is stationary (*arrows*). (*From* Tirkes T, Menias CO, Sandrasegaran K. MR imaging techniques for pancreas. Radiol Clin North Am 2012;50(3):385; with permission.)

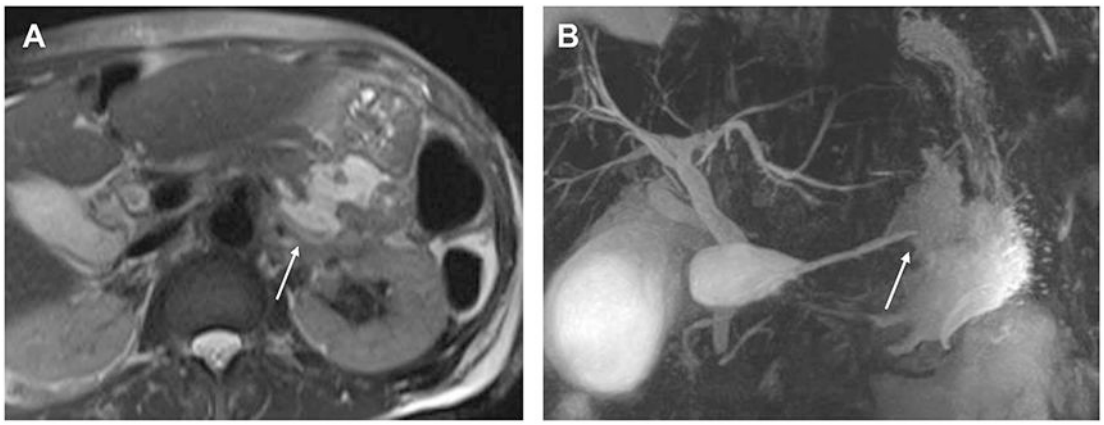

Fig. 3.

(*A*) T2-weighted axial image of a patient after a motor vehicle collision showing a fluid collection transecting the tail of the pancreas (*arrow*). (*B*) Maximum intensity projection MRCP image depicting the pancreatic duct (*arrow*) communicating with the fluid collection in this patient with a transected pancreas.

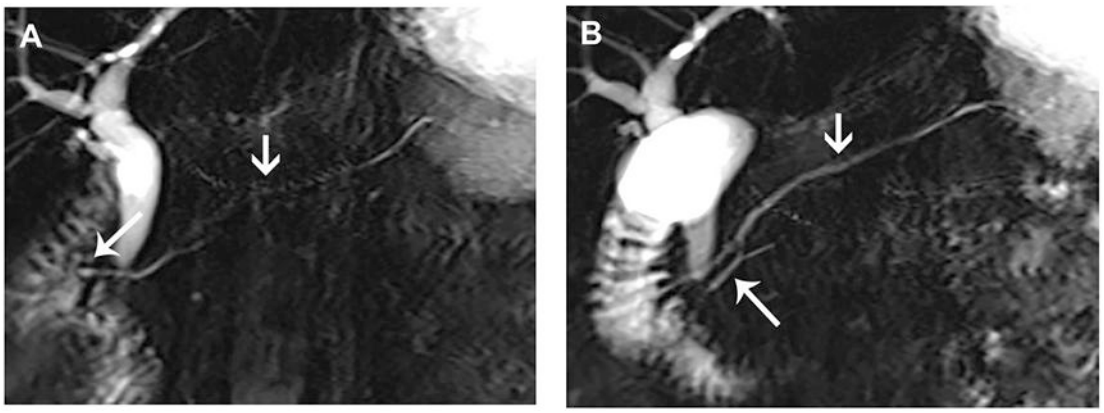

Fig. 4.

A 47-year-old patient with chronic abdominal pain. (*A*) Coronal thick-slab MRCP image shows effacement of the main pancreatic duct in the region of the body (*short arrow*). There is evidence of pancreas divisum as the main pancreatic (dorsal) duct (*long arrow*) drains into the duodenum at the minor papilla. (*B*) This image was obtained in the same patient following injection of secretin. There is complete visualization of the main pancreatic duct (*short arrow*), which appears unremarkable. The ventral duct, which was not visible before secretin (*long arrow*), is also visible.

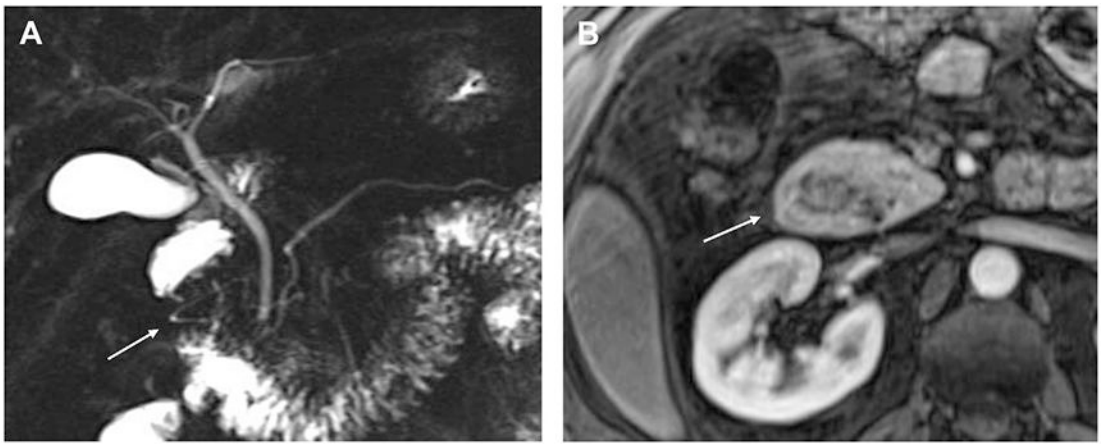

Fig. 5.

(*A*) Secretin-enhanced MRCP with abnormal looping configuration of the pancreatic duct with concurrent narrowing of the lumen of the descending duodenum (*arrow*). (*B*) T1-weighted contrast-enhanced, fat-suppressed, image demonstrates enhancing pancreatic parenchyma surrounding the descending duodenum compatible with annular pancreas (*arrow*).

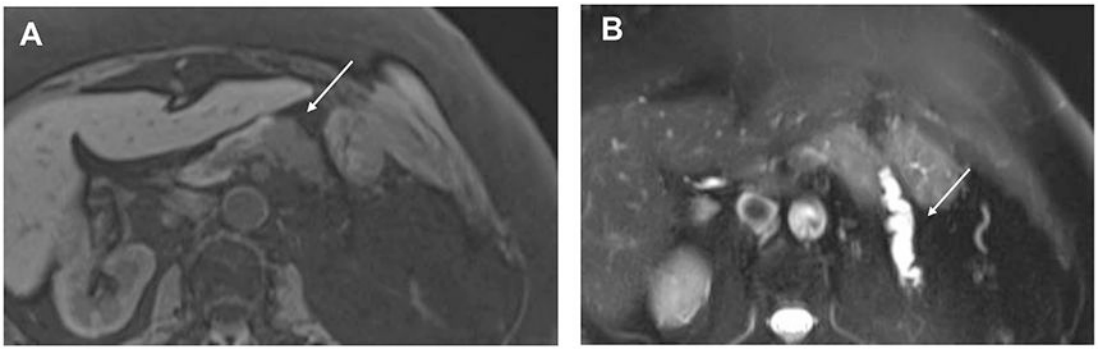

Fig. 6.

(*A*) Unenhanced T1-weighted image of the pancreas demonstrating the difference between the normal hyperintense signal of the pancreatic head and the ovoid hypointense signal of a PDAC (*arrow*). (*B*) Axial T2-weighted image demonstrates the mass with abrupt cutoff and upstream dilatation of the main pancreatic duct (*arrow*).

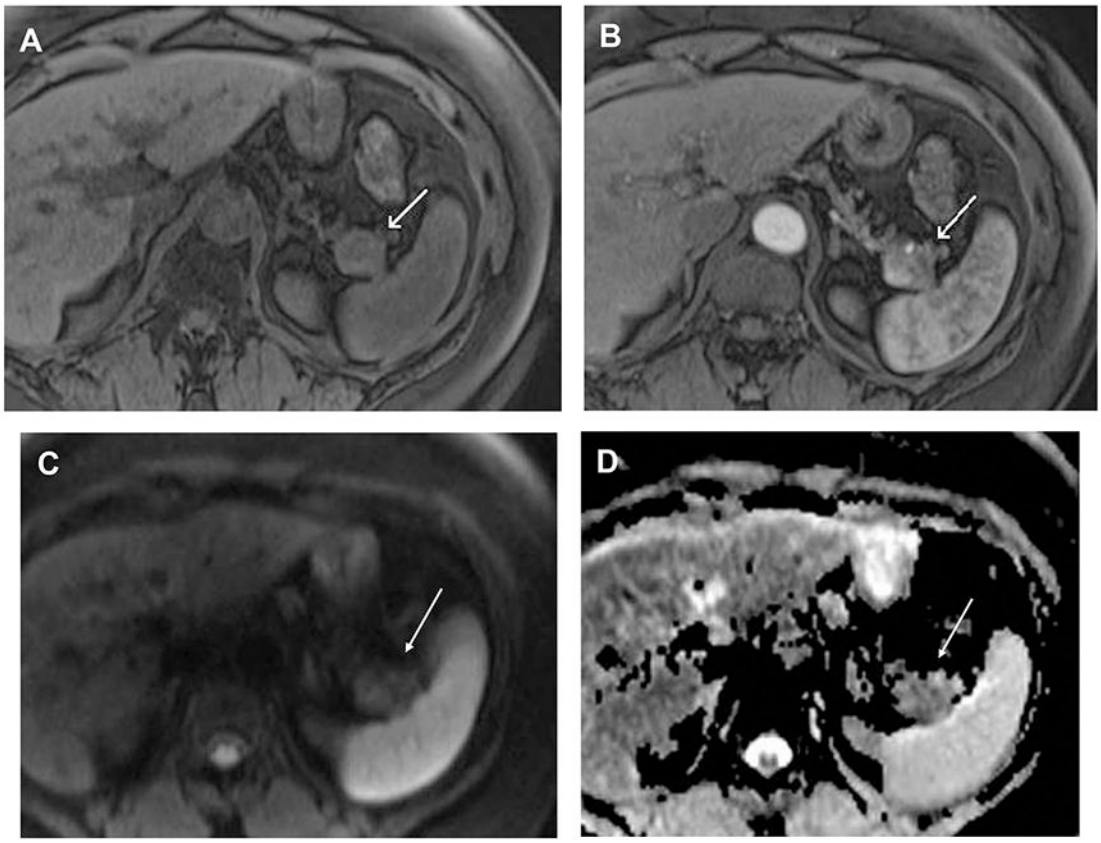

Fig. 7.

(*A*) Axial unenhanced, T1-weighted, fat-suppressed, image demonstrating a mass in the tail of the pancreas (*arrow* in *A*–*D*). (*B*) Axial contrast-enhanced T1-weighted, fat-suppressed, image showing arterialphase enhancement consistent with a pancreatic neuroendocrine tumor. (*C*) DWI and (*D*) ADC map through the tail of the pancreas showing restricted diffusion.

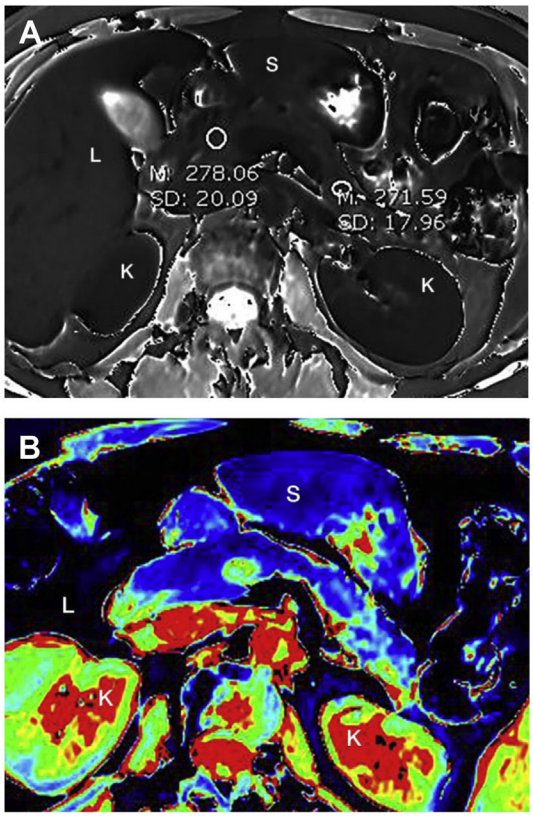

Fig. 8.

T_1 relaxometry provides quantitative evaluation of the pancreas. (*A*) Axial grayscale T1 map obtained at 1.5 T has round region-of-interest measurements of the pancreas. The mean T_1 in the pancreatic head measures 278 milliseconds, and the mean T_1 in the tail measures 271 milliseconds. (*B*) Axial T1 map in a color-scale format. The intensity of the pancreatic signal can be visually assessed by color of the scale. K, kidneys; L, liver; S, stomach.

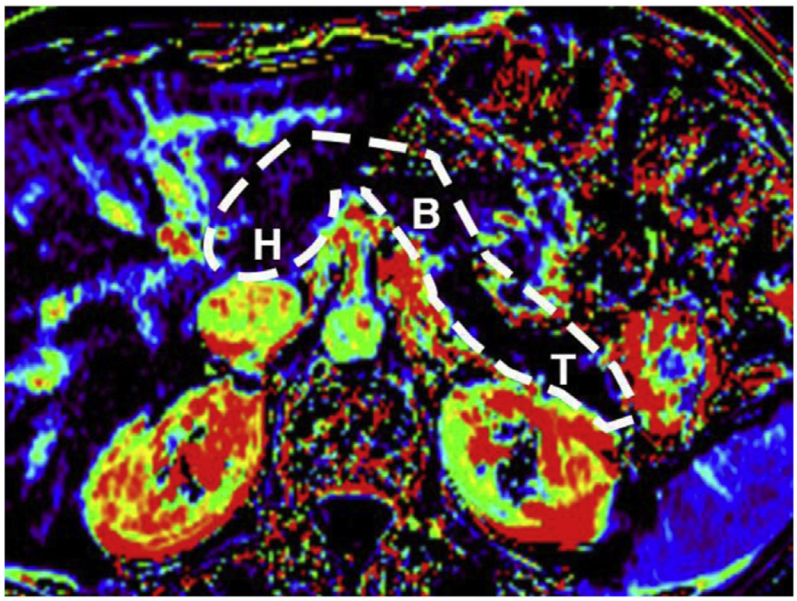

Fig. 9.

ECV imaging of the CP. ECV imaging technique uses T_1 maps obtained before and after MR contrast enhancement. This axial color map image depicts calculated ECV fraction. B, body; H, head; T, tail of the pancreas.

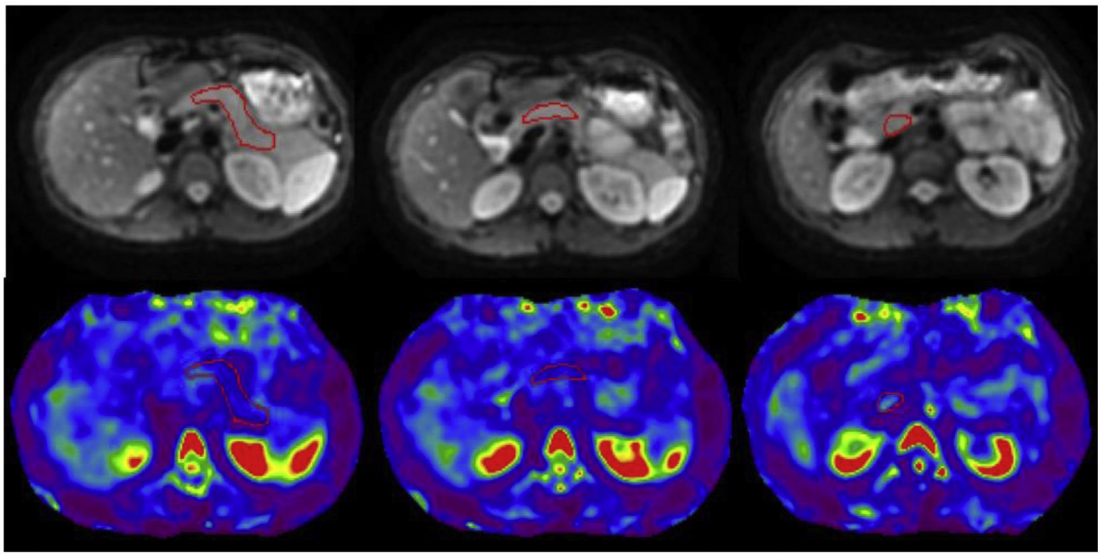

Fig. 10.

MRE of the pancreas in a normal healthy volunteer. MRE was performed at 40 Hz using a 3D echo planar imaging sequence with slice thickness of 3 mm. Top row demonstrates magnitude images at the level of the tail, body, and head of the pancreas. Bottom row shows corresponding stiffness maps (scale 0–8 kPa). The red outline represents the region of interest drawn in different parts of the pancreas. The mean stiffness is 1.15 kPa (range 1.02–1.18 kPa). (*Courtesy of* S. Venkatesh, MD, Rochester, MN.)

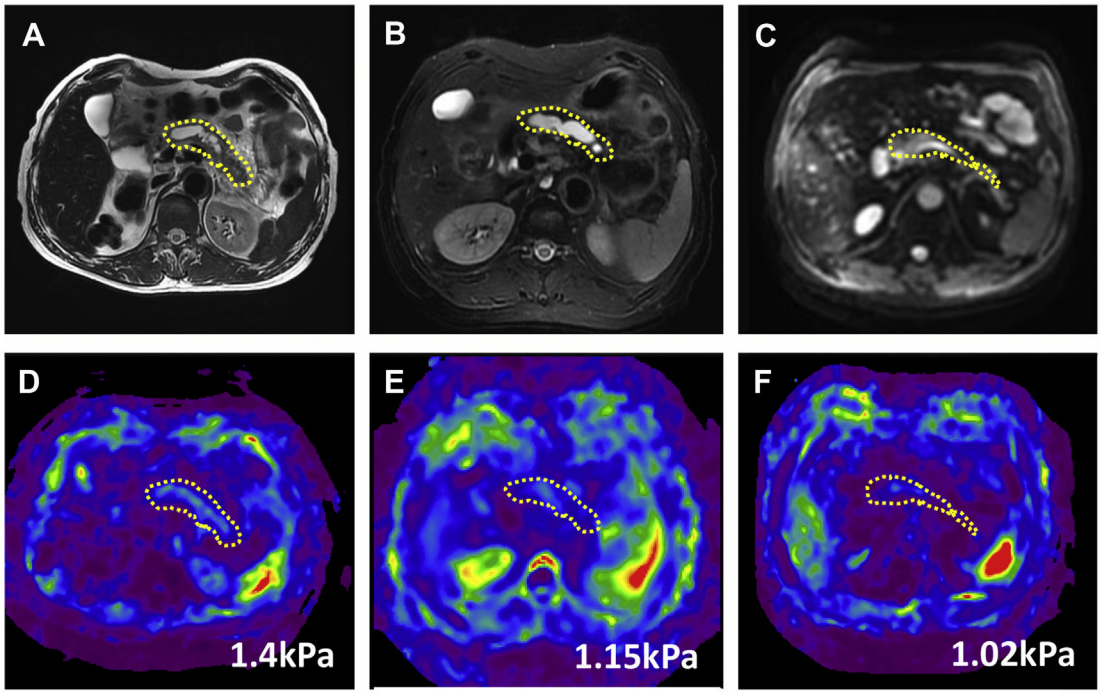

Fig. 11.

MRE in CP. (*A*, *B*) T2-weighted images and (*C*) magnitude image in 3 patients with CP and (*D*–*F*) their corresponding level MRE stiffness maps. Note the dilated pancreatic duct (*A* and *B*), and the severe atrophy of the pancreas (*C*). The mean pancreas stiffness is elevated in the first example; however, in the other 2 patients, the mean stiffness is within normal limits and actually lower in the patient with severe pancreatic atrophy (*C*, *F*). (The *yellow dotted lines* outline the pancreas). (*Courtesy of* S. Venkatesh, MD, Rochester, MN; and Y. Shi, MD, Shengjing Hospital, Shenyang, China.)

Table 1

Parameters for pancreatic imaging on 1.5-T MR imaging scanners

	3D SPGR DIXON	**T2 2D SSFSE**	**T2 2D STIR**	**T2 2D SSFSE**	**MRCP 2D Slab**	**MRCP 3D**	**MRCP Secretin**	**3D SPGR FS**
Plane of acquisition	Axial	Axial	Axial	Coronal	Coronal	Coronal	Coronal	Axial
TR/TE (ms)	7.47/4.76 (in), 2.38 (out)	1100/90	2900/132 (TI 150)	1100/90	2000/755	2500/691	2000/756	5.17/2.52
Flip angle (degree)	10	130–50	180	130	180	Variable	1	12
ST/SG	3.4/−	4.0/4.0	7	4.0/4.0	40	1/−	40	3.0/−
NEX	1	1	1	1	1	2	1	1
RBW	290	475	250	476	300	372	300	300
Phase direction	A to P	A to P	A to P	R to L	R to L	R to L	R to L	A to P
Echo train length	1	160	33	192	320	189	256	1
Matrix	256 × 120	256 × 192	256 × 180	256 × 192	256 × 256	384 × 346	256 × 256	256 × 144
FOV	400	360	360	360	290	350	290	360
Respiration	BH	BH	BH	BH	BH	Navigator	BH	BH
Fat saturation	No	No	IR	No	Fat sat	Fat sat	Fat sat	Fat sat
Concatenation	1	3	4	3	8	1	1	1
Parallel imaging	2	No	No	No	No	3	No	2
Scan time (min:s)	0:12	0:44	0:58	0:31	0:18	3:55	0.03 (9:58)	0:18 (3:28)

These are guidelines for use on a 1.5-T MR imager. The names of sequences and parameter values may vary with different MR vendors.

Abbreviations: 3D SPGR DIXON, 3D nonfat-saturated spoiled gradient-echo sequence for chemical shift imaging; 3D SPGR FS, fat-saturated 3D spoiled gradient-echo T1-weighted sequence for postcontrast; BH, breath-hold; Concatenation, number of interleaved acquisitions or number of breath-holds; Fat sat, spectral selective fat saturation; FOV, field of view in millimeters; Navigator, navigator monitored respiratory triggering (see text); NEX, number of excitations; PI, parallel imaging, where PI is used; the number given is the acceleration factor. PI is typically performed with GRAPPA (GeneRalized Auto-calibrating Partially Parallel Acquisition); Phase direction, A to P is anterior to posterior, R to L is right to left; RBW, receiver bandwidth in Hertz/pixel; Scan time, scan time in minutes. The time given in parentheses is the total scan times for performing the secretin-enhanced MRCP series and the 3 postGd series; Secretin, presecretion and postsecretion MRCP as described in the text; SSFSE, half single-shot fast spin-echo sequence; ST/SG, slice thickness and slice gap in millimeters. 2D MRCP and secretin MRCP slabs are single slabs of 40 mm thickness. 3D sequences do not have slice gap.

Table 2

Parameters for pancreatic imaging on 3.0 T MR imaging scanners

Parameter	3D SPGR DIXON	T2 2D SSFSE	T2 2D SSFSE	MRCP 2D Slab	MRCP 3D	MRCP Secretin	3D SPGR FS
Plane of acquisition	Axial	Axial	Coronal	Coronal	Coronal	Coronal	Axial
TR/TE (ms)	5.45/2.45 (in), 3.68 (out)	2000/96	2000/97	4500/622	2400/719	4500/746	4.19/1.47
Flip angle (degree)	9	150	150	160	Variable	180	9
ST/SG	4.0/—	5/5.2	4/4.4	40/—	1.2/—	40/—	2.6/—
NEX	1	1	1	1	2	1	1
RBW	500 or 780	780	780	383	318	161	350
Phase direction	AP	AP	R to L	R to L	R to L	R to L	AP
Echo train length	1	168	256	307	101	288	1
Matrix	320 × 224	320 × 224	320 × 256	384 × 306	380 × 380	384 × 306	308 × 210
Field of view	400	380	350	300	380	300	400
Respiration	BH	BH	Navigator	BH	Navigator	BH	BH
Fat saturation	No	SPAIR	No	Fat Sat	SPAIR	Fat Sat	SPAIR
Concatenation	1	4	1	8	1	1	1
Parallel imaging	2	2	3	2	2	2	2
Scan time (min:s)	0:16	1.08	1:50	0:36	3:54	0.04 (9.56)	0:19 (3:19)

These are guidelines for use on a 3.0 T MR imager. The names of sequences and parameter values may vary with different MR vendors.

The time given in parentheses is the total scan times for performing the secretin-enhanced MRCP series and the 3 post-Gd series; 2D MRCP and Secretin MRCP slabs are single slabs of 40 mm thickness. 3D sequences do not have slice gap.